

A Stretchable and Flexible Cardiac Tissue–Electronics Hybrid Enabling Multiple Drug Release, Sensing, and Stimulation

Ron Feiner, Lior Wertheim, Danielle Gazit, Or Kalish, Gal Mishal, Assaf Shapira, and Tal Dvir*

Replacement of the damaged scar tissue created by a myocardial infarction is the goal of cardiac tissue engineering. However, once the implanted tissue is in place, monitoring its function is difficult and involves indirect methods, while intervention necessarily requires an invasive procedure and available medical attention. To overcome this, methods of integrating electronic components into engineered tissues have been recently presented. These allow for remote monitoring of tissue function as well as intervention through stimulation and controlled drug release. Here, an improved hybrid microelectronic tissue construct capable of withstanding the dynamic environment of the beating heart without compromising electronic or mechanical functionality is reported. While the reported system is enabled to sense the function of the engineered tissue and provide stimulation for pacing, an electroactive polymer on the electronics enables it to release multiple drugs in parallel. It is envisioned that the integration of microelectronic devices into engineered tissues will provide a better way to monitor patient health from afar, as well as provide facile, more exact methods to control the healing process.

demand for donor hearts far exceeds their availability.^[4] According to the American Heart Association, CVD accounts for one out of every seven deaths in the US.^[4] One of the most common cardiac pathologies leading to a need for a heart replacement is a myocardial infarction (MI). An MI occurs when a coronary artery supplying blood to the heart muscle is obstructed, leading to a state of hypoxia in the cardiac muscle. This state of hypoxia, if not resolved quickly, leads to tissue necrosis and the eventual formation of a non-contracting, nonconductive fibrotic scar tissue.^[5] While the goal of cardiac tissue engineering is mostly focused on the treatment of MI, other forms of CVD, such as conduction and rhythm disorders can also benefit from replacement of a part of the ventricular wall.

1. Introduction

The field of tissue engineering aims to create functional replacements for damaged tissues and organs in order to provide a solution for the worldwide shortage in organ donations.^[1–3] Specifically, the rise in cardiovascular disease (CVD) in the western world has created a situation, in which the

Cardiac tissue engineering is based on seeding cells on or within a biomaterial scaffold. This scaffold is meant to allow the cells to organize into a functional tissue with capabilities closely resembling those of native tissues.^[6] Once a functional tissue is engineered, it can be implanted on the heart to replace the fibrotic scar tissue. Implanted cardiac patches have already shown to improve the symptoms of an MI compared to nontreated hearts.^[7,8]

Recent works in the field have shown advances in engineered tissue function. This was done for example by improving scaffold conductivity,^[9,10] by mimicking the native structure of the cardiac microenvironment^[11,12] and by integrating growth factors into the scaffold, which are slowly released to affect the cells or the host.^[2,13] While major strides have been made in the field, there remain major obstacles to overcome. One such obstacle is the inflammatory response that follows tissue implantation and how to reduce it.^[14] Modern cardiac pacemaker leads contain anti-inflammatory drug eluting systems in order to minimize immune rejection.^[15] While controlled release systems for various growth factors have been widely described in the field of tissue engineering, there is still a need to reduce immune response following tissue implantation. Another major issue in the field deals with how to monitor tissue function and integration after implantation. Such methods to monitor tissue function may allow minimizing surgical intervention and reduce the response time once a pathology has been detected.

Recent advances in the field of flexible electronics have brought forth the integration of flexible electronic systems into engineered tissues.^[16–19] These flexible electronic systems

R. Feiner, D. Gazit, O. Kalish, Dr. A. Shapira, Prof. T. Dvir
School for Molecular Cell Biology and Biotechnology
Tel Aviv University
Tel Aviv 69978, Israel
E-mail: tdvir@tauex.tau.ac.il

R. Feiner, L. Wertheim, Prof. T. Dvir
The Center for Nanoscience and Nanotechnology
Tel Aviv University
Tel Aviv 69978, Israel

L. Wertheim, G. Mishal, Prof. T. Dvir
Department of Materials Science and Engineering
Tel Aviv University
Tel Aviv 69978, Israel

Prof. T. Dvir
Sagol Center for Regenerative Biotechnology
Tel Aviv University
Tel Aviv 69978, Israel

 The ORCID identification number(s) for the author(s) of this article can be found under <https://doi.org/10.1002/sml.201805526>.

DOI: 10.1002/sml.201805526

are extremely delicate and capable of easily folding and adapting to the complex surfaces of the body. Recent works have described the development of electronic meshes delicate enough for syringe injection.^[19,20] However, one other key parameter in the design of an implantable device is its ability to withstand the mechanical deformations involved in the dynamic motions of the body, such as the contractions of the heart or peristaltic activity of the digestive system. This feat is crucial as it could reduce the chances of device failure, delamination and immune rejection due to a mechanical mismatch.^[21,22]

In recent studies, our lab has shown the capability to use an electronic system to monitor engineered tissue function from

within, and if needed, intervene by supplying electrical stimulation and controlled drug release.^[18,23–25] In this work, we set to improve upon existing systems by fabricating a hybrid electronic tissue construct capable of easily withstanding the tensile stress and mechanical deformations applied by the beating heart, without compromising mechanical or electrical performance. In addition, we report on a controlled drug release system capable of releasing multiple anti-inflammatory medications from an electroactive polymer deposited on the device (**Figure 1**). On-demand drug release is demonstrated for several different drugs and control over the amount of drug released is shown. Finally, we demonstrate the integration of our system into a biomaterial and its capability to serve as a hybrid scaffold

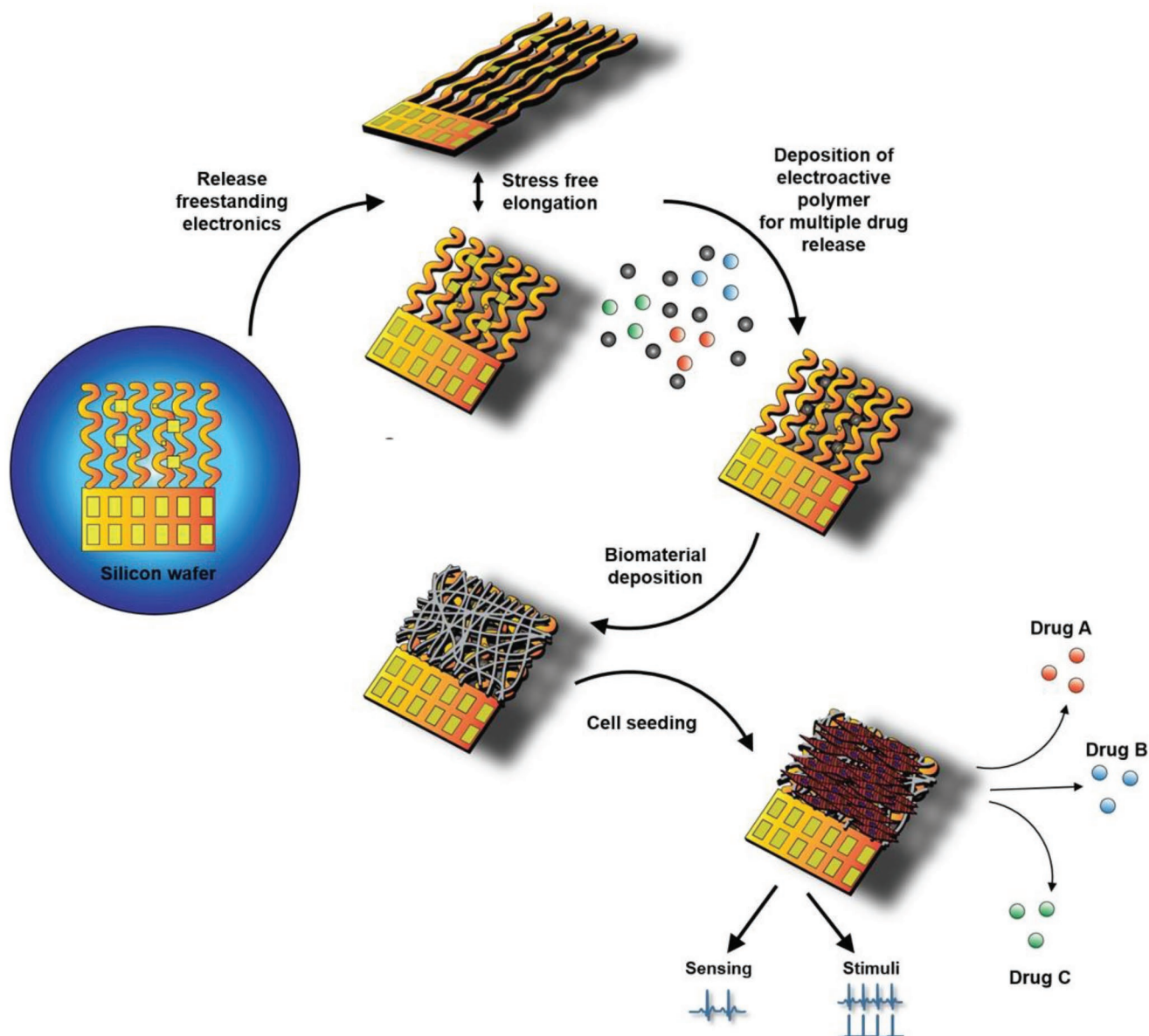


Figure 1. Schematic illustration of the hybrid microelectronic tissue concept. The device is manufactured on a silicon wafer in 2D and is then released to yield freestanding porous electronics. Drug loaded electroactive polymer layers are deposited on the central electrodes followed by electrospinning of PCL-gelatin nanofibers to create a scaffold for cell seeding. The resulting hybrid tissue can then be used to monitor tissue function, intervene through electrical stimulation and controlled release of drugs.

for cardiac tissue engineering, while providing real time monitoring and intervention functions.

2. Results and Discussion

2.1. Device Fabrication

In order to fabricate completely freestanding devices, they first need to be fabricated onto a silicon wafer in 2D (Figure 2A). A layer of polymethylmethacrylate (PMMA) is spin coated onto the wafer as a sacrificial layer that can be removed later to release the device (Figure 2B). A 5 μm thick bottom layer of polyimide (PI) is then spin coated onto the wafer (Figure 2C) followed by electron beam evaporation of a 200 nm layer of gold on top of a 10 nm chromium adhesion layer (Figure 2D). Photolithography and wet etching is then used to define the metal electrodes (Figure 2E). A second, 5 μm thick layer of PI is then spin coated onto the wafer placing the metal electrodes in the mechanically neutral plane and providing passivation for the gold electrodes (Figure 2F). Photolithography and reactive ion etching are then used to define the device by first exposing the electrode pads and then by definition of the entire device (Figure 2G and H). Finally, the wafer is placed in acetone to etch away the bottom PMMA layer, resulting in a completely freestanding device (Figure 2I).

Figure 3A shows an image of the fabricated device before its release from the wafer. The mesh like device consists of six separate serpentine filaments connected at one side to a large rectangle that serves as a connector to external data acquisition and stimulation devices. On the second side, it is connected to another PI filament intended to hold them all together. These filaments are designed in a serpentine architecture in order to enable extension while minimizing stress. Ten gold electrodes were defined onto the device. The two extreme filaments composing the mesh were almost completely covered by large counter electrodes to aid in both stimulation and drug release functions. Four large, 1 mm² electrodes were distributed on the middle filaments. These large electrodes were designated for electroactive polymer deposition and controlled drug release, as well as for tissue stimulation (Figure 3B). The large exposed surface area in these electrodes allows for a larger amount of electroactive polymer to be deposited on them, increasing the amount of drugs that can be stored and released. Four other, 150 μm electrodes are placed, two on each of the remaining filaments between the counter electrodes and the middle filaments (Figure 3C). These smaller electrodes were designed for noninvasive recording of extracellular potentials. Due to their smaller size, these electrodes will come in contact with a smaller number of cells, thus increasing the sensitivity of the recordings and reducing the signal to noise ratio. Figure 3D shows a scanning electron microscopy image of the edge of the exposed gold electrode pad. The bottom PI layer can be seen below the edge of the gold electrode pad and a second PI layer surrounding it providing passivation for the remainder of the gold electrode. This ensures that the cells contact the electrodes only at specific locations, minimizing background noise and allowing for specific point stimulation.

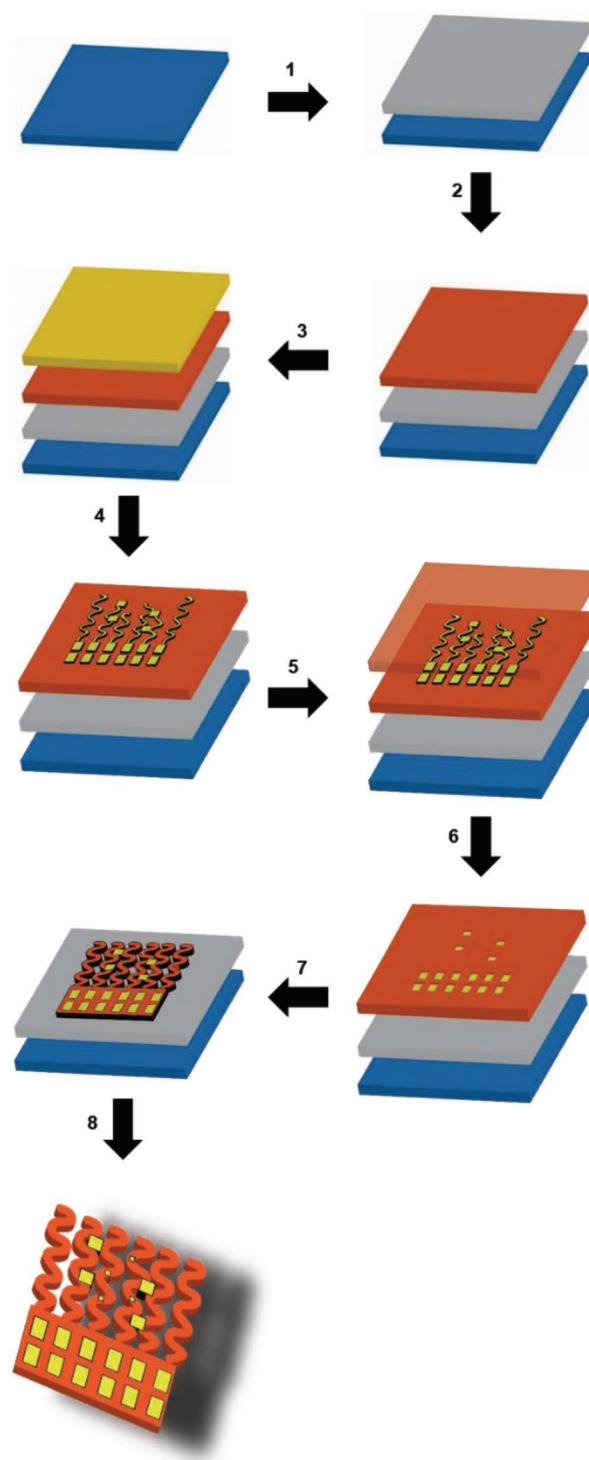


Figure 2. Schematic illustration of the fabrication process. Step 1: Spin coat sacrificial PMMA layer. Step 2: Spin coat bottom, polyimide layer, 5 μm thick. Step 3: Evaporate a thin 10 nm layer of chromium followed by a 200 nm layer of gold. Step 4: Define gold electrodes using photolithography and wet etching. Step 5: Spin coat a second, 5 μm thick polyimide layer for upper passivation. Step 6: Perform photolithography and reactive ion etching to expose electrode pads. Step 7: Perform photolithography and reactive ion etching to define complete device. Step 8: Release device by etching away the sacrificial PMMA layer in acetone.

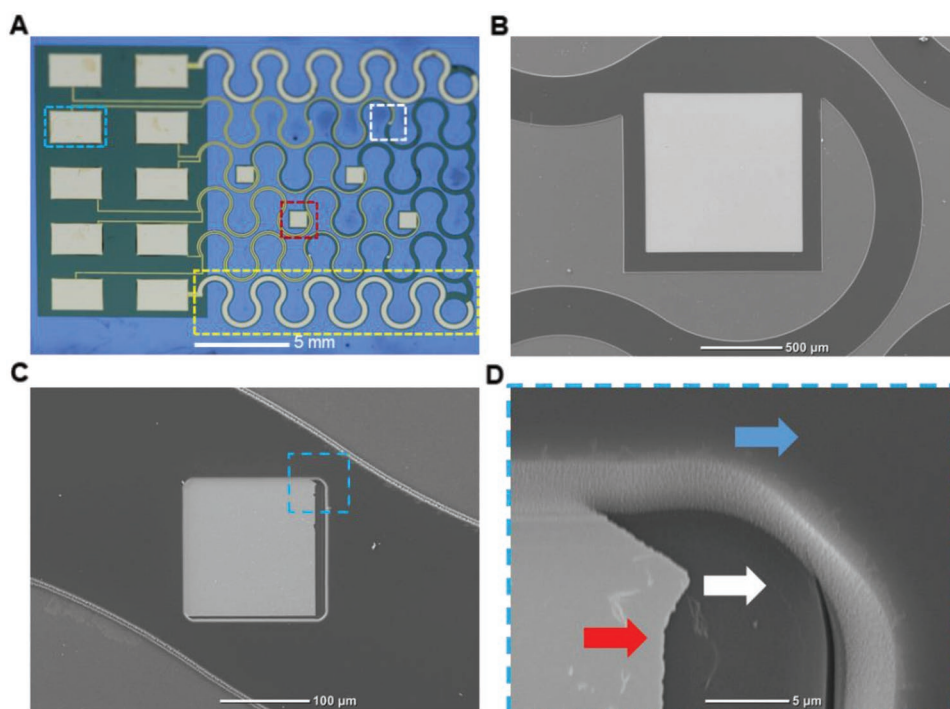


Figure 3. The electronic device. A) Macro image of the complete fabricated device. A large drug release electrode is highlighted in red, a small recording electrode is highlighted in white, a large serpentine counter electrode is highlighted in yellow and a pad for external data acquisition and stimulation is highlighted in cyan. B) Scanning electron microscopy image of the large electrode for drug release. C) Scanning electron microscopy image of the small, recording electrode used for sensing cardiac cell extracellular signals. D) A Zoom-in image of the highlighted area in (C), showing the bottom polyimide layer (white arrow), gold electrode pad (red arrow), and top polyimide layer (blue arrow).

2.2. Electrical Properties Characterization

In order to evaluate the performance of the device following its release from the wafer, resistance was measured over multiple electrodes, before and after removal of the sacrificial layer. The measurements showed that there was no increase in resistance following release (Figure 4A). In order to emulate the contractions of the human heart and evaluate the device's capability to withstand physical manipulations, the device was cycled 1000 times from 5% to 20% strain in the y direction. Cardiac sarcomeres can extend up to 20% and volume changes between the systolic and diastolic states of the heart can reach up to 10%.^[26] Resistance measurements of the freestanding devices a function of tensile strain showed no significant changes until the point of failure at $\approx 140\%$ strain (Figure 4B). Resistance was also measured as a function of cyclic tensile strain between 5% and 20%. No significant changes in resistance were measured over 1000 cycles. (Figure 4C).

As the electrodes in the device are designed to form a close connection with the cells of the engineered tissue, the device was covered with the adhesive protein fibronectin, which contains the cell adhesion motif: arginine-glycine-glutamate (RGD). This is done in order to increase cell attachment to the gold electrodes. Cyclic voltammetry measurements showed that the device was electrochemically active, both before and after coating, as could be seen by the oxidation waves measured within a ferri/ferrocyanide solution (Figure 4D). This shows that the adsorbed protein modified electrode activity, but did not block it. Impedance measurements across a wide range of

frequencies in cell culture medium, and at room temperature revealed low levels, indicating on the potential of the devices to serve as sensors under physiological conditions (Figure 4E).

2.3. Mechanical Properties Characterization

As the purpose of our device is to serve as a scaffold for the engineering of a cardiac tissue, we sought to evaluate its ability to withstand mechanical extension similar to that exhibited by the human heart. As a first step to assess the stress state that developed on the device due to deformation, finite element analysis (FEA) simulation was performed. Figure 5A depicts the results of the FEA and shows that when simulated strain reached up to 50%, stress was well distributed throughout the device (Movie S1, Supporting Information). High stress values were only predicted at the extremities and not on the entire width of the filament. Images of a manually extended freestanding device are shown in Figures 5B and 5C. These images show that the device can withstand relatively large deformations without failure. The serpentine filaments could be seen extending similar to the FEA model predictions in Figure 5A. When examined by a mechanical tester no significant increase in stress for up to $\approx 75\%$ strain was observed (Figure 5D). This was in accordance with the FEA model. At about 75% strain, stress started to increase and at $\approx 130\%$ reached the tensile strength of ≈ 2.35 MPa and the device failed. In order to measure fatigue, the devices were cycled from 5% to 20% strain over 1000 cycles, the exhibited stress remained low and

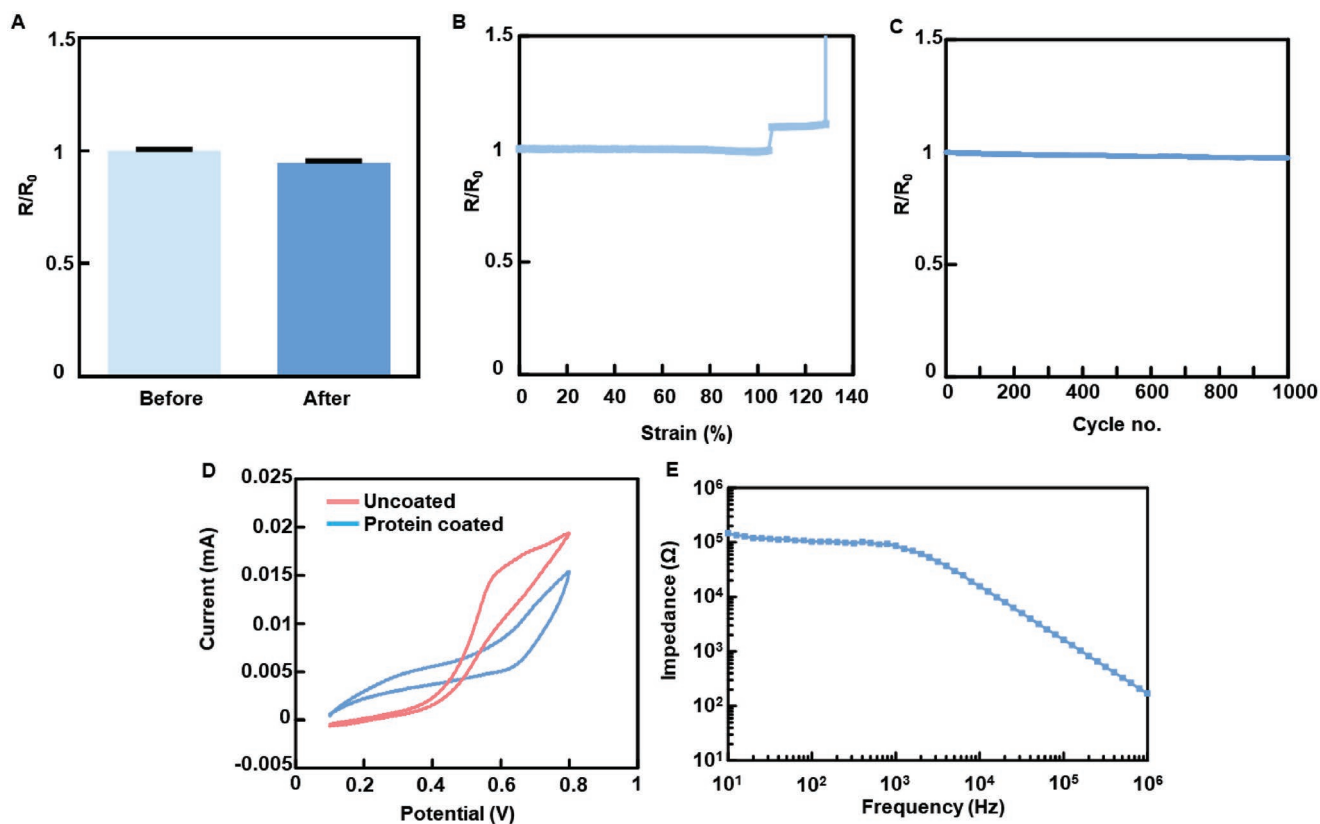


Figure 4. Electrical characterization of the device. A) Resistance before and after release from the silicon wafer. B) Resistance measured as a function of tensile strain. C) Resistance measured over 1000 cycles of tensile extension between 5% and 20%. D) Cyclic voltammogram of the device before and after fibronectin coating. E) Impedance characterization of electrodes evaluated in cell culture medium.

only reached 10% of the measured stress at failure (Figure 5E), indicating on the robustness of the electronics. Once we have characterized our device, our next step was to assess its functionality in terms of drug release.

2.4. On-Demand Drug Release

Immune rejection is one of the major risks faced in cardiac tissue engineering and in the implantation of biomedical devices in general.^[3] Once a foreign tissue or device is implanted, an immune reaction will be mounted against it. This reaction poses a risk to the implanted device and the tissue as the immune reaction can lead to device degradation and tissue death. One of the methods to reduce the risk of an immune reaction is by administering anti-inflammatory drugs following implantation. These can increase the odds of implant integration with the host and cell survival.^[21]

Polypyrrole is an electroactive polymer that can be used to coat conductive surfaces through the oxidation of its monomer, pyrrole.^[27,28] In the coating process, a positively charged film of polypyrrole is deposited over the electrode. Negatively charged molecules are trapped within the film by electrostatic bonds to the pyrrole backbone. Once the polymer film has been deposited, the electrostatic bonds can be broken by reduction through the underlying electrode. The negatively charged molecules will then diffuse out of the polymer film into its environment (Figure 6A,B).^[28–30]

Previous works done in our lab have shown the ability of polypyrrole to serve as a platform for controlled drug release from freestanding flexible devices integrated within engineered tissues.^[24,25] In these works, dexamethasone was released as a single load from the polypyrrole film. While useful, a single release may not be efficient for long-term treatment and immune abatement. In addition, while dexamethasone is a commonly used anti-inflammatory agent, instances of adverse reaction to its administration have been reported.^[31] In order to improve our ability to control the outcome of tissue implantation we set to both improve the drug release profile from polypyrrole and expand the variety of drugs that can be released. These are used here as a proof of concept for negative drug release from polypyrrole.

We first deposited a layer of drug-loaded polypyrrole onto the large electrodes in the devices by a process of chronopotentiometry. The polymerization process was performed in a 3-electrode setup with the application of currents ranging between 0.25 and 1 mA for 5–10 min in a solution containing only pyrrole monomers and the added drug. (Figure 6C,D). The loading process can be optimized to control the amount of drug loaded into the film. This is due to the correlation between the amount of charge delivered for the polymerization process and the thickness of the resulting polypyrrole film.^[25] Release was performed in phosphate buffered saline and the drugs were quantified using spectrophotometry with typical absorbance wavelengths. The properties of each drug, including the size,

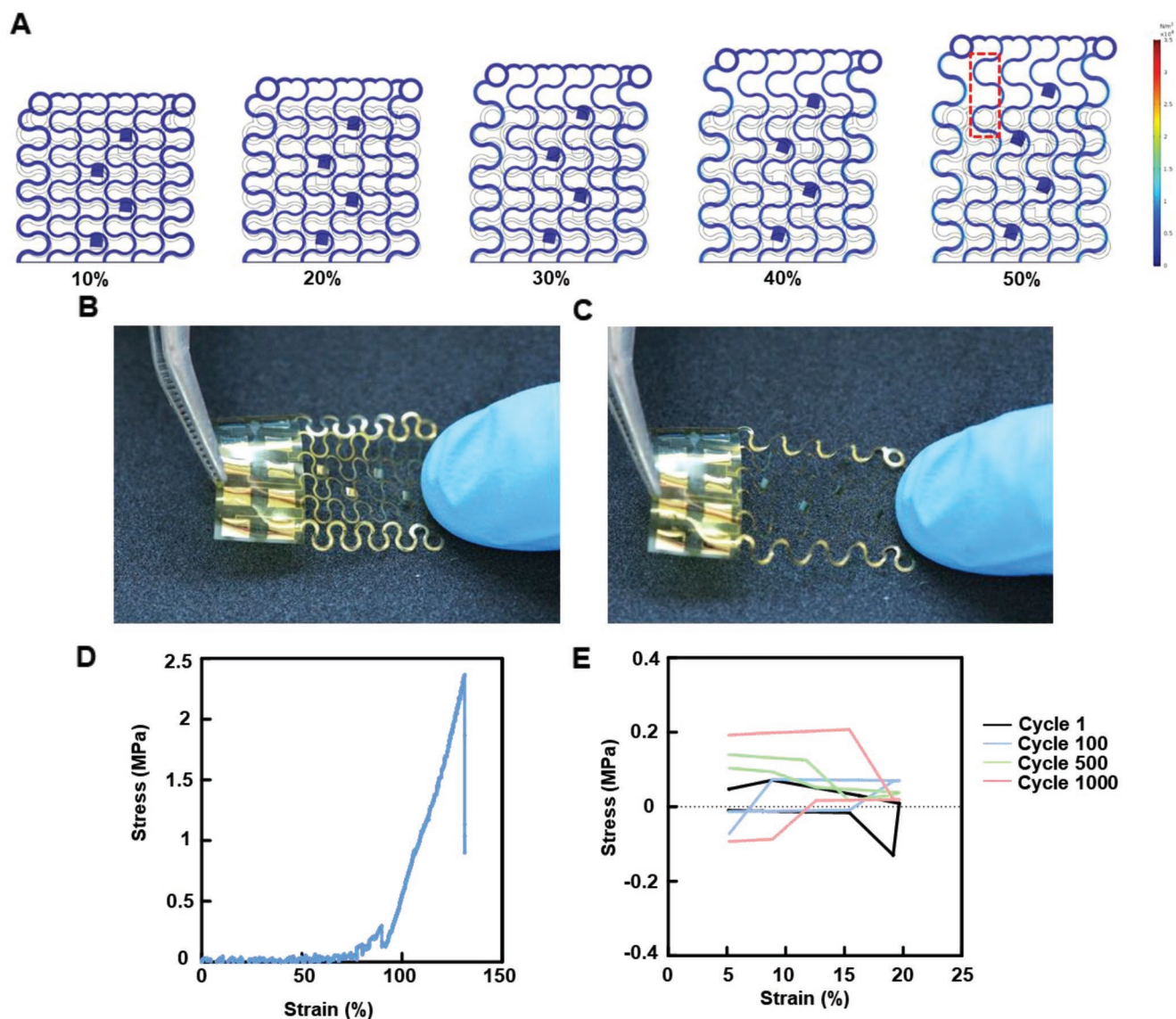


Figure 5. Characterization of the mechanical properties of the device. A) Finite element analysis simulation of tensile stress on the device. B) Free-standing device without manipulation. C) Free-standing device after manual extension. D) Typical stress–strain curve resulting from the tensile test performed on the device. E) Typical stress–strain curve of the cyclical tensile stress performed on the device.

structure and charge, influence its release profile and therefore, the amount of charge needed for release of different molecules may vary. First, dexamethasone was released from the device in an on-off profile. Three cycles of drug release were performed by applying a constant current of 1 mA for a period of 10 min with 30 min after each cycle in which a small amount to no drug was released (Figure 6E).

Next, we sought to release a nonsteroidal anti-inflammatory drug (NSAID). We chose indomethacin, which is commonly used to reduce a serious inflammation. The same drug release profile was achieved as with dexamethasone, with three repeating on-off release cycles. However, here, a constant current of 0.1 mA was used (Figure 6F). As a third drug, we chose acetylsalicylic acid (ASA), one of the most commonly used drugs, commonly known as aspirin. ASA is given following an MI to improve prognosis by reducing inflammation, as well as

preventatively to reduce the risk of an MI by inhibiting blood clot formation.^[32] In addition, ASA is used to treat pericarditis, an inflammation of the pericardium, commonly reported following open chest surgery.^[33] Using the electronics, ASA release in three repeating on-off cycles was achieved, by providing a constant current of 1 mA (Figure 6G). In addition, we set to understand the relationship between the strength and length of the applied current used for drug release and the amount of drug released (Figure 6H,I). A linear relationship between the amount of released ASA and the applied current (Figure 6H) or the length of reduction reaction (Figure 6I) was found. This means that there is a direct correlation between the amount of charge transferred to the polypyrrole film and the amount of released drug. The same correlation can be drawn to the amount of drug loaded within the device, which can be increased or decreased according to the amount of charge

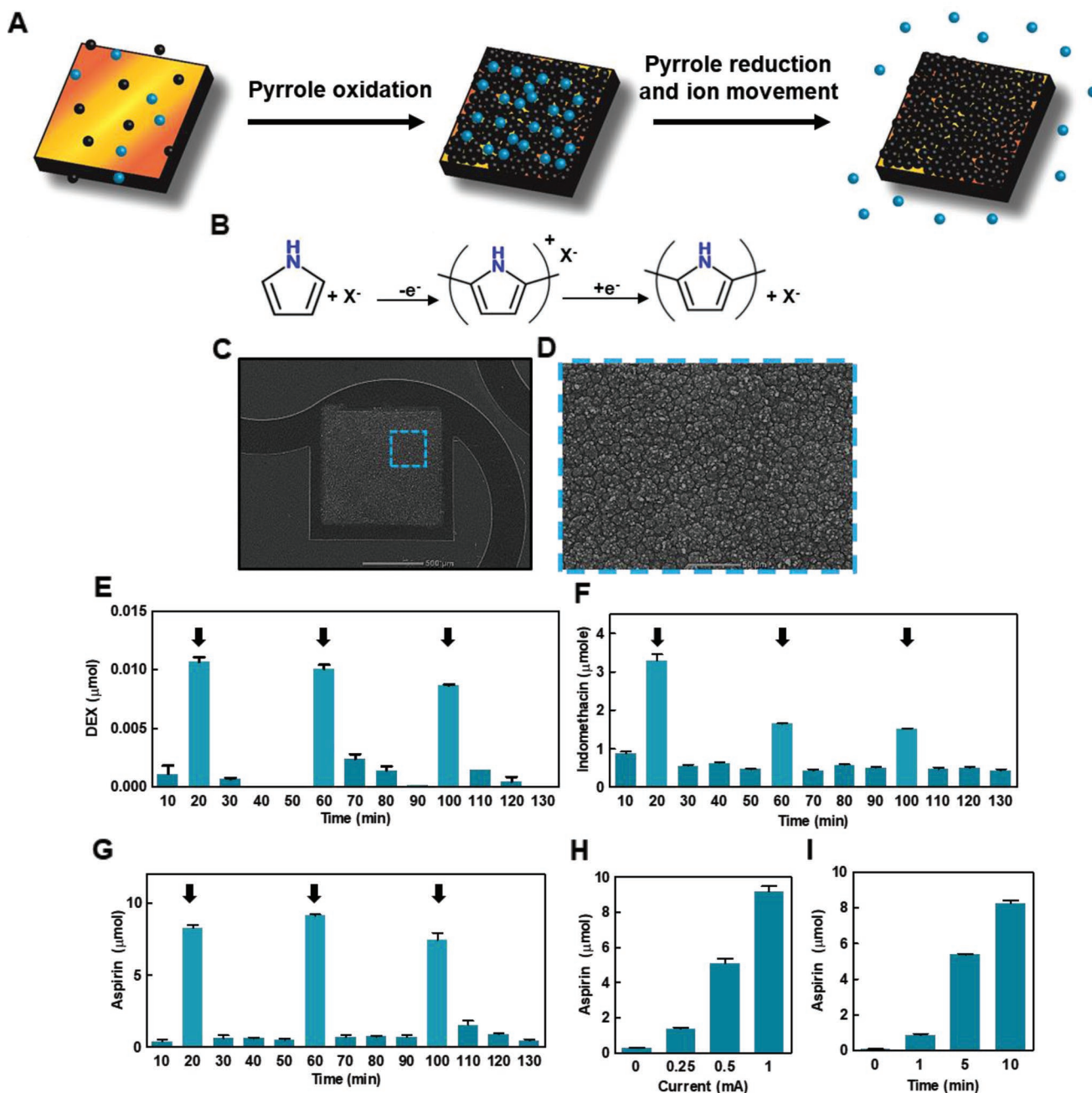


Figure 6. Controlled drug release from the device. A) Schematic representation of drug loading and release from the system. The pyrrole monomers (black spheres) are oxidized, leading to the creation of a polypyrrole film containing the negatively charged drug (blue spheres). On polypyrrole reduction, the electrostatic bonds between the polymer and the drugs are broken, leading to the release of the drug. B) Chemical reaction for polypyrrole polymerization and subsequent reduction and drug release. C) Scanning electron microscopy image of a large drug release electrode with a layer of drug-loaded polypyrrole deposited on it. D) Zoomed-in image of the highlighted area in C showing a close up of the polypyrrole layer. Drug release from the device showing an on-off release profile: E) dexamethasone, F) Indomethacin, and G) Aspirin. Arrows represent a period of current injection. H) Aspirin release as a function of applied current in milliamperes. I) Aspirin release as a function of time with the application of a 1 mA current.

transferred in the polymerization process and the needs of the treatment. This is in accordance with previous works describing drug release from polypyrrole films.^[27,28] While we have focused here on three specific drugs, other negatively charged drugs could be incorporated into the polypyrrole film. For example, glutamate that exhibits a protective effect on cardiac

function following MI could be used,^[34] and amiodarone, a common antiarrhythmic medication could be released to treat conduction disorders.^[35] Other examples of molecules released from polypyrrole films include adenosine triphosphate, glutamate and dopamine.^[28,30] The choice of drugs is of course not limited to CVD treatment. Any type of anionic molecule could

potentially be released from this system and allow for a tightly controlled release profile.

As the electronic system is intended to regulate engineered tissue function, we next sought to integrate it with a biomaterial scaffold for cardiac tissue engineering.

2.5. Integration of Nanofibrous Scaffold and Characterization

In order to engineer a functional cardiac patch, cardiac cells are seeded within a 3D scaffold. A successful scaffold should promote cell attachment that will lead to the formation of cell–cell

and cell–matrix interactions. These lead to cell elongation, alignment and cardiac muscle bundle formation. The most straightforward method to achieve this is by mimicking the natural fibers of the heart matrix.^[1] In order to mimic the natural collagen fibers in the heart, we used electrospinning. Thus, a composite scaffold of polycaprolactone and gelatin fibers was deposited on the electronic mesh. The resulting fibers had an average diameter of 250 ± 51 nm resembling in size to the endomyial fibers of the heart, which wrap individual cells (Figure 7A,B). These fibers connect to the plasma membrane of the cells through integrins to form a tight interaction between the ECM and the cytoskeleton of the cell.^[36] The meshwork of

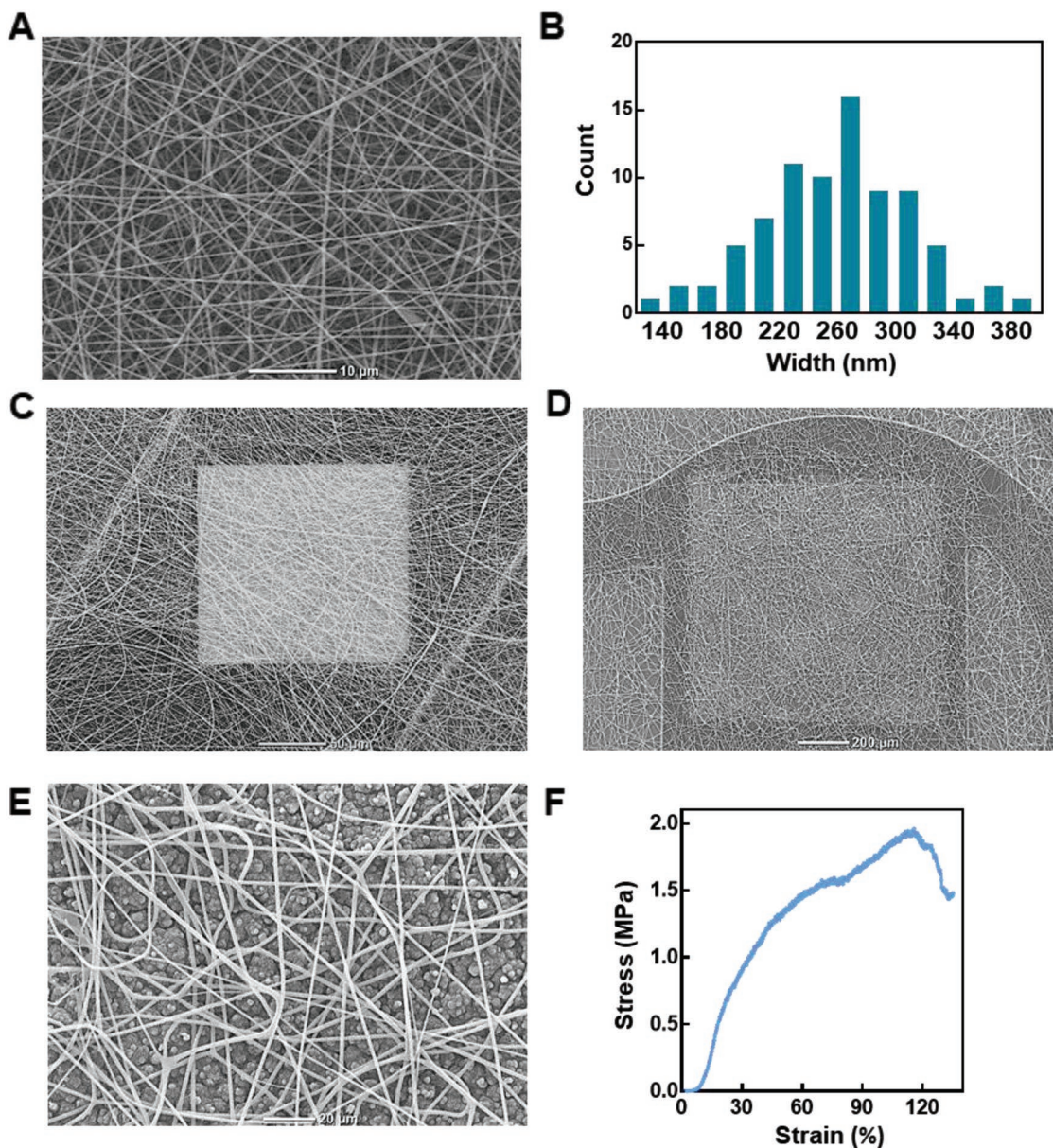


Figure 7. Electronics-biomaterial scaffold hybrid. A) Scanning electron microscopy image of the electrospun PCL-gelatin nanofibers. B) Histogram showing the distribution of nanofiber diameter. C) Scanning electron microscopy image of the electrospun nanofibers on the small recording electrode. D) Scanning electron microscopy image of the electrospun nanofibers covering the drug-loaded polypyrrole layer, which is deposited on the large drug release electrode. E) Zoom-in on the electrospun nanofibers covering the polypyrrole layer. F) Typical stress–strain curve resulting from the tensile test performed on the hybrid device.

fibers covered the entire device; creating a 3D porous scaffold, allowing cell penetration to both the small recording electrodes (Figure 7C) and the large stimulating electrodes (Figure 7D). When deposited over a layer of drug-loaded polypyrrole, the fiber network was porous enough to allow drug diffusion into the cellular microenvironment. Additionally, the electrospun fibers provided mechanical support to the polypyrrole film in a case of unwanted delamination (Figure 7D,E). When the stress–strain behavior of the composite scaffold was tested, it showed a shorter stress free phase, followed by a steady rise in stress as a function of strain until reaching a tensile strength of ≈ 2 MPa, similar to that of the pristine device before failure (Figure 7F). This behavior is in accordance with previously reported pristine PCL-gelatin fiber scaffolds.^[37] Other types of biomaterials can also be applied to the electronic device and be used as potential scaffolds. For example, we have recently reported on the development of a thermoresponsive hydrogel derived from decellularized omentum.^[12,38] This hydrogel can be applied as a scaffold onto our device by way of drop casting as it is liquid in room temperature and solidifies into a gel when exposed to physiological temperatures (Figure S1, Supporting Information). After gelation, the hydrogel formed a much thicker fibrillar network of collagenous nanoscale fibers, covering the device (Figures S2 and S3, Supporting Information). However, the hydrogel scaffold limited the ease of elongation of our device as can be seen in Figure S4 (Supporting Information). Hence, we chose to continue with cell seeding on the electrospun fiber network.

2.6. Cardiac Tissue Organization and Function

In order to assess our composite device's capability to promote cardiac tissue organization, freshly isolated neonatal rat ventricular cardiomyocytes were seeded onto it. Confocal microscopy images of the cells on the device showed homogenous distribution throughout the scaffold, attaching to the nanofibers, the polyimide substrate and the gold electrodes themselves (Figure 8A). When observed under higher magnification, elongated cardiomyocytes could be seen, with a high aspect ratio and massive actinin striation (Figure 8B). When the viability of the cardiac cells in the tissue was evaluated over 7 d by measuring their metabolic activity, no reduction in cardiac cell viability was measured as can be seen in Figure S5 (Supporting Information). Together, these results indicate on the formation of a viable and functional cardiac tissue with hallmarks of the native myocardium.^[8] In order to evaluate the device's capability to monitor cardiac cell function, extracellular potentials were recorded from within the engineered cardiac tissue, showing a contraction rate of ≈ 0.8 Hz (Figure 8C). The recorded extracellular potentials exhibited a shape and width characteristic of neonatal ventricular cardiomyocytes (Figure 8D).^[39]

Finally, we sought to demonstrate our system's capability in intervening with the contraction rate of the engineered tissue. This could prove useful when the tissue is contracting nonsynchronously, if the contraction pace is not sufficient, or if conduction disorders appear in the tissue or heart. We recorded the contractions of the engineered tissue without intervention and then paced the tissue at 1 Hz, followed by a 2 Hz stimulation.

When stimulation was applied, the tissue contracted synchronously and responded directly to the applied stimulation regimen (Figure 8E).

3. Conclusions

In this work, we have reported on the fabrication of a free-standing, flexible and stretchable multielectrode device. We have provided mechanical and electrical evidence of our system's ability to withstand continuous physical deformations similar to those exhibited on a beating heart. We have shown that our system is capable of accommodating multiple drug release systems within, and shown our ability to control the type of drug released, the time and duration of the release and the amount of drug that is released. In addition, biomaterial deposition and cell seeding have proven our ability to engineer a functional cardiac tissue and create a hybrid electronic cardiac patch. The function of this hybrid patch can be monitored in real time from afar and intervention could be provided in the form of electrical stimulation or drug release when needed.

The field of tissue engineering aims at replacing damaged tissues and organs to overcome the current shortage in available organ donations. By integrating electronics into engineered tissues, it will become possible to improve the standard of care for patients receiving tissue and organ replacements. In this work, we have demonstrated the integration of electronics into an engineered cardiac patch and the release of anti-inflammatory drugs. However, this can be possible with a variety of other tissues, whether excitable or not. By integrating different types of controlled release systems, positively charged molecules could be released, as has been demonstrated with growth factor release from the negatively charged chondroitin sulfate.^[25] Future work will focus on providing evidence for the feasibility of these drug release systems to function within an in vivo setting and ascertain their safety and effectiveness. In addition, a variety of different sensors could be integrated into these types of devices to sense heat, pH,^[17] and mechanical motions^[40] as well as sense the concentrations of molecules, such as nutrients, inflammation markers, breathing gasses or signaling molecules.^[41] Future devices will be capable of withstanding mechanical strain in all directions and can benefit from a design based on the contraction vectors of the cardiac muscle.

Hybrid systems, such as the one reported here demonstrate a more sophisticated approach toward tissue engineering. An approach in which the physician would be able to monitor convalescence and intervene from afar, minimal surgical intervention would be necessary and the amount of human error could be minimized, as all data collection, and responses would be performed by onboard processors, such as those of cardiac pacemakers.

4. Experimental Section

Device Fabrication: The process begins with spin coating a layer of poly(methylmethacrylate) (PMMA 495 A2, MicroChem, USA) at 3000 RPM onto a silicon wafer (University wafers, USA) followed by baking at 180 °C for 60 s. The first polyimide (PI2525, HD microsystems,

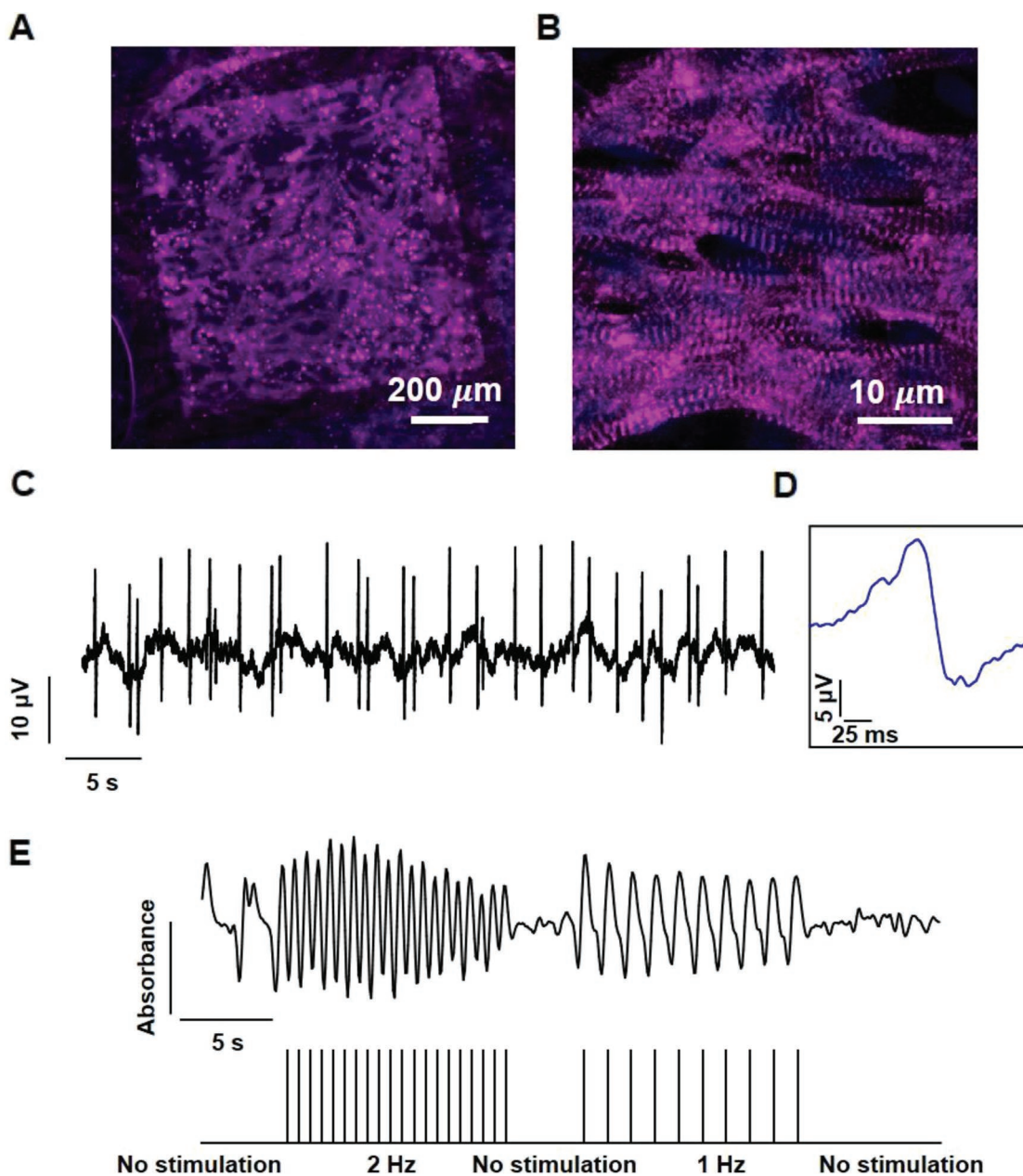


Figure 8. Tissue assembly and function within the microelectronic scaffold. A) Confocal microscope image showing the assembled cardiac tissue within the biomaterial–electronics hybrid. A large drug release electrode can be seen in the background. B) A Zoomed-in image of cardiac cells revealing cell elongation and massive striation. Sarcomeric actinin in pink, nuclei in blue. C) Extracellular potential recordings collected from an electrode within the tissue. D) Zoomed-in extracellular potential recording, showing a typical signal recorded from ventricular cardiomyocytes. E) Quantification of tissue contraction as a function of stimulation through the microelectronic device. The stimulation pattern is presented in the lower part.

Japan) substrate layer is then deposited by spin coating at 3000 RPM to yield a 5 μm thick layer, which is then baked at 225 $^{\circ}\text{C}$ for 6 h in an oven. Next, electron beam evaporation is used to deposit a 10 nm thick layer of chromium for adhesion and a 200 nm thick layer of gold (VST e-beam evaporator (VST, Petah Tikva, Israel)). Au (99.999%) was evaporated from a tungsten boat at $1\text{--}3 \times 10^{-6}$ Torr at a deposition rate of 2.5 A s^{-1} . An etching mask is then deposited. This is achieved by spin coating AZ1518 photoresist (MetalChem Ltd., Israel) at 3000 RPM, followed by baking at 115 $^{\circ}\text{C}$ for 90 s, exposure and development in AZ 726 developer. Subsequent etching of gold and chromium is performed using gold and chromium etch, respectively, to define the

gold electrodes followed by stripping of the remaining photoresist using acetone and isopropanol. Next, a second PI substrate layer is deposited by spin coating at 3000 RPM to yield a total thickness of 10 μm . It is then baked at 225 $^{\circ}\text{C}$ for 6 h in an oven. This layer insulates the gold electrodes and places them in the neutral mechanical plane. An etching mask to define the exposed gold electrode pads is prepared by spin coating AZ4620 (MetalChem Ltd., Israel) at 3000 RPM, baking at 115 $^{\circ}\text{C}$ for 90 s, exposure and development in AZ 400K developer (1:2 in double distilled water (DDW)). Reactive ion etching is used to expose the electrode pads in the PI top layer (200 mTorr, 20 sccm O_2 , 150 W for ≈ 40 min). These two steps are repeated to define the open web design

of the device. Next, a double layer of AZ 4620 is deposited, followed by an 80 min reactive ion etching process. Finally, the devices are released from the silicon wafer by incubation in acetone for ≈20 min to dissolve the bottom PMMA layer.

Scanning Electron Microscopy: Samples were mounted onto aluminum stubs with conductive paint and were sputter-coated with an ultrathin (150 Å) layer of gold in a Polaron E5100 coating apparatus (Quorum Technologies). The samples were viewed under a JCM-6000PLUS NeoScope benchtop scanning electron microscope (JEOL USA, Inc.).

Cyclic Voltammetry: Devices were placed in a solution containing 10×10^{-3} M potassium hexacyanoferrate (II) and potassium hexacyanoferrate (III) (Sigma-Aldrich) in Milli-Q water of $18 \text{ M}\Omega \text{ cm}^{-1}$ resistivity. Cyclic voltammograms were recorded between 0.1 and 0.8 V at a scan rate of 50 mV s^{-1} between a device electrode, a platinum counter electrode and an Ag/AgCl reference electrode using a Bio-Logic SP-150 potentiostat. Protein coated devices were incubated in a solution of $10 \mu\text{g mL}^{-1}$ fibronectin (Biological Industries, Kibbutz Beit-Haemek, Israel) in phosphate buffered saline (PBS) for 24 h and then washed in DDW three times.

Impedance Spectroscopy: Impedance spectroscopy: Devices were placed in a phosphate buffered saline solution. A large drug release electrode ($1 \text{ mm} \times 1 \text{ mm}$) was chosen as the working electrode, an external ($1 \text{ cm} \times 1 \text{ cm}$) platinum electrode as the counter electrode with a distance of 5 mm, and Ag/AgCl as a reference electrode using a Bio-Logic SP-150 potentiostat. A scan rate of 10 mV s^{-1} was used across a frequency range of 10^1 – 10^6 Hz.

Electrical Resistance Measurements: All measurements of conductivity were performed using a DMM-7510 multimeter (Keithley Instruments, Cleveland, OH) using a two probe setup.

Finite Element Analysis: The geometries of the chip were designed using AutoCAD (Autodesk, California, USA). The testing geometries in stereolithography format were imported directly into the Structural Mechanics Module in COMSOL Multiphysics (COMSOL Group, Stockholm, Sweden). The models were meshed using 784 413 tetrahedral elements for 3D analysis. Material properties were assumed homogenous and isotropic. The Young's modulus (3.1 GPa) used in the analysis was taken from the PI2525 datasheet. The Poisson's ratio was assumed 0.34. The solution was found using a stationary solver at an axial strain of 10%, 20%, 30%, 40%, and 50% in the y-direction.

Mechanical testing: Devices were tested using a model LS1 tensile testing instrument (Lloyd Instruments, Ltd.) with a 5 N load cell at a rate of 5 mm min^{-1} .

Drug Release from Polypyrrole Films: Drug containing PPy films were grown potentiostatically onto the device electrodes using a Bio-Logic SP-150 potentiostat. The dexamethasone electro-synthesis solution consisted of 0.2 M Pyrrole (Alfa Aesar, Ward Hill, MA) and 0.02 M dexamethasone 21 phosphate disodium salt (Sigma-Aldrich, used as received) in Milli-Q water of $18 \text{ M}\Omega \text{ cm}^{-1}$ resistivity. The Indomethacin electro-synthesis solution consisted of 0.2 M Pyrrole and 0.01 M Indomethacin (Sigma-Aldrich) in acetonitrile. The acetylsalicylic acid electro-synthesis solution consisted of 0.2 M Pyrrole (Alfa Aesar, Ward Hill, MA) and 0.02 M acetylsalicylic acid (Sigma-Aldrich) in Milli-Q water. The films were synthesized by applying a constant current of 0.1 mA for indomethacin and 1 mA for acetylsalicylic acid and dexamethasone each for 10 min between the drug release electrode and the counter electrode. For drug release experiments, the counter and working electrodes were reversed. The amount of released DEX, ASA and indomethacin was quantified by absorbance at 242, 298, and 318 nm, respectively, using an infinite M200 Pro plate reader (TECAN).

Nanofiber Scaffold Fabrication: Nanofibers were fabricated by electrospinning as previously described.^[37] Briefly, 10% gelatin (Sigma, St. Louis, MO) and 10% PCL (Sigma) were separately dissolved in 2,2,2-trifluoroethanol (Acros Organics, Geel, Belgium) overnight at room temperature. The following day, the solutions were mixed in a ratio of 1:1 and the polymer solution was delivered through a stainless steel 20G capillary at a feeding rate of 0.5 mL h^{-1} using a syringe pump (Harvard apparatus, Holliston, MA). A high voltage power supply (Glassman high voltage Inc., High Bridge, NJ) was used to apply a 10 kV potential

difference between the capillary tip and the collector, positioned 10 cm beneath the tip. First, a layer of nanofibers was deposited onto an aluminum foil, then the device was placed onto the deposited film and another layer of fibers was deposited. Finally, after letting the devices dry and the solvent evaporate, the devices were cut out with the deposited scaffold layers.

Omentum Hydrogel Formation: Omentum decellularization: Porcine omenta from healthy pigs (Kibbutz Lahav, Israel), were washed with PBS followed by incubation in a hypotonic buffer (10×10^{-3} M Tris, 5×10^{-3} M ethylenediaminetetraacetic acid (EDTA) and 1×10^{-6} M phenylmethanesulfonyl-fluoride (PMSF), pH 8.0) for 1 h. Next, tissues were frozen and thawed three times using the same buffer. The tissues were washed gradually with 70% ethanol and 100% ethanol for 30 min each. Lipids were extracted by three, 30 min washes of 100% acetone, followed by 24 h incubation in a 60/40 (v/v) hexane: acetone solution (solution was replaced three times during incubation). The defatted tissue was washed in 100% ethanol for 30 min and incubated overnight at 4°C in 70% ethanol. Then, the tissue was washed four times with PBS (pH 7.4) and incubated in 0.25% Trypsin-EDTA (Biological Industries) overnight. The tissue was washed thoroughly with PBS and incubated in 1.5 M NaCl for 24 h (solution was replaced three times), followed by washing in 50×10^{-3} M Tris (pH 8.0), 1% triton-X100 (Sigma) solution for 1 h. The decellularized tissue was washed in PBS followed by double distilled water and then frozen (-20°C) and lyophilized.

After lyophilization, decellularized omentum was ground into powder (Wiley Mini-Mill, Thomas Scientific, Swedesboro, NJ). Dry, milled omentum was enzymatically digested for 96 h at room temperature with stirring, in a 1 mg mL^{-1} solution of pepsin (Sigma, 4000 U mg^{-1}) in 0.1 M HCl. Subsequently, pH was adjusted to 7.4 using DMEM/F12 (Biological industries). The final concentration of decellularized omentum in the titrated solution was 1% (w/v).

Cardiac Cell Isolation, Seeding and Cultivation: Cardiac cells were isolated according to Tel Aviv University ethical use protocols as previously described.^[9] Briefly, left ventricles of 0–3 d old neonatal Sprague–Dawley rats (Envigo, Israel) were harvested, and cells were isolated using six cycles (30 min each at 37°C) of enzyme digestion with collagenase type II (95 U mL^{-1} ; Worthington, Lakewood, NJ) and pancreatin (0.6 mg mL^{-1} ; Sigma-Aldrich) in Dulbecco's modified Eagle Medium (DMEM, $\text{CaCl}_2 \cdot 2\text{H}_2\text{O}$ (1.8×10^{-3} M), KCl (5.36×10^{-3} M), $\text{MgSO}_4 \cdot 7\text{H}_2\text{O}$ (0.81×10^{-3} M), NaCl (0.1 M), NaHCO_3 (0.44×10^{-3} M), NaH_2PO_4 (0.9×10^{-3} M)). After each round of digestion, cells were centrifuged (600G, 5 min) and resuspended in culture medium composed of M-199 supplemented with 0.6×10^{-3} M $\text{CuSO}_4 \cdot 5\text{H}_2\text{O}$, 0.5×10^{-3} M $\text{ZnSO}_4 \cdot 7\text{H}_2\text{O}$, 1.5×10^{-3} M vitamin B12, 500 U mL^{-1} Penicillin and 100 mg mL^{-1} streptomycin, and 0.5% (v/v) fetal bovine serum (FBS) (Biological industries, Israel). To enrich the cardiomyocyte population, cells were suspended in culture medium with 5% FBS and pre-plated twice (45 min). Cell number and viability were determined by a hemocytometer and trypan blue exclusion assay. Cells were then centrifuged and resuspended in 1% hydrogel at a concentration of 150×10^6 cells mL^{-1} . Prior to cell seeding, the devices were incubated in a solution of $10 \mu\text{g mL}^{-1}$ of fibronectin (Biological Industries, Kibbutz Beit-Haemek, Israel) in PBS for 24 h in order to improve cell adhesion to the device and then washed in DDW three times. The hydrogel was then placed onto the device and allowed to solidify for 30 min at 37°C . Following gel solidification, cell culture medium contacting 5% FBS was added and refreshed every other day.

Immunostaining: Cell constructs were fixed and permeabilized in 100% cold methanol for 10 min, washed three times in PBS, and then blocked for 1 h at room temperature in DMEM-based buffer containing 2% (v/v) FBS. Then, the samples were washed three times in PBS. Cardiac tissues were incubated with a primary mouse anti- α -sarcoplasmic actinin antibody (1:500) (Sigma-Aldrich), washed three times, and incubated for 1 h with a secondary Alexa Fluor 647-conjugated goat antimouse antibody (1:250) (Jackson). For nuclei detection, the cells were incubated for 3 min with Hoechst 33258 (1:100) (Sigma) and were washed three times. Samples were visualized using a scanning laser confocal microscope (Nikon Eclipse Ni).

Stimulation and Analysis: Constructs were imaged using an inverted fluorescent microscope (Nikon Eclipse TI). Videos were acquired with an ORCA-Flash 4.0 digital complementary metal-oxide semiconductor (CMOS) camera (Hamamatsu Photonics) at 100 frames s⁻¹ using NIS-Elements software (Nikon). Tissue movements were measured using ImageJ (NIH). Stimulation was performed using a Multichannel Systems STG-4002 stimulus generator. Pacing was performed by applying 1–3 V, 50 ms long pulses at 1–2 Hz.

Extracellular Potential Recordings: The devices were connected to an AM systems differential AC amplifier Model 1700 and then to a USB X series multifunction data acquisition system (National Instruments). Extracellular potentials were recorded using LabView Express software.

Fiber Diameter Analysis: SEM images were taken and images were analyzed using ImageJ software ($n = 98$).

Statistical Analysis: Data are presented as means \pm SEM. Differences between samples were assessed by a Student's *t*-test. All analyses were performed using GraphPad Prism version 6.00 for Windows (GraphPad Software). $p < 0.05$ was considered significant.

Supporting Information

Supporting Information is available from the Wiley Online Library or from the author.

Acknowledgements

T.D. Acknowledges support from the European Research Council (ERC) starting grant 637943, the Slezak Foundation, the Israeli Science Foundation (700/13), and the Israel Ministry of Science, Technology and Space (3-14412). R.F. was supported by the Clore scholarship, the Marian Gertner Institute of Medical Nanosystems and the Argentinian friends of Tel Aviv University. The work is part of the doctoral thesis of R.F. at Tel Aviv University.

Conflict of Interest

The authors declare no conflict of interest.

Keywords

cardiac patches, cardiac tissue engineering, controlled release, electrospun fiber scaffolds, microelectronics

Received: December 27, 2018

Revised: February 17, 2019

Published online: March 5, 2019

- [1] T. Dvir, B. P. Timko, D. S. Kohane, R. Langer, *Nat. Nanotechnol.* **2011**, *6*, 13.
- [2] A. Shapira, R. Feiner, T. Dvir, *Int. Mater. Rev.* **2016**, *61*, 1.
- [3] S. Fleischer, R. Feiner, T. Dvir, *Curr. Opin. Biotechnol.* **2017**, *47*, 23.
- [4] W. G. MEMBERS, E. J. Benjamin, M. J. Blaha, S. E. Chiuvé, M. Cushman, S. R. Das, R. Deo, S. D. de Ferranti, J. Floyd, M. Fornage, *Circulation* **2017**, *135*, e146.
- [5] a) J. Leal, R. Luengo-Fernández, A. Gray, S. Petersen, M. Rayner, *Eur. Heart J.* **2006**, *27*, 1610; b) S. Rohr, *Heart Rhythm* **2009**, *6*, 848.
- [6] S. Fleischer, R. Feiner, T. Dvir, *Regener. Med.* **2017**, *12*, 275.
- [7] a) T. Dvir, A. Kedem, E. Ruvinov, O. Levy, I. Freeman, N. Landa, R. Holbova, M. S. Feinberg, S. Dror, Y. Etzion, *Proc. Natl. Acad. Sci. USA* **2009**, *106*, 14990; b) W.-H. Zimmermann, I. Melnychenko, G. Wasmeier, M. Didié, H. Naito, U. Nixdorff, A. Hess, L. Budinsky, K. Brune, B. Michaelis, *Nat. Med.* **2006**, *12*, 452; c) J. S. Wendel, L. Ye, R. Tao, J. Zhang, J. Zhang, T. J. Kamp, R. T. Tranquillo, *Stem Cells Transl. Med.* **2015**, *4*, 1324.
- [8] W.-H. Zimmermann, K. Schneiderbanger, P. Schubert, M. Didie, F. Munzel, J. Heubach, S. Kostin, W. Neuhuber, T. Eschenhagen, *Circ. Res.* **2002**, *90*, 223.
- [9] M. Shevach, B. M. Maoz, R. Feiner, A. Shapira, T. Dvir, *J. Mater. Chem. B* **2013**, *1*, 5210.
- [10] a) M. Shevach, S. Fleischer, A. Shapira, T. Dvir, *Nano Lett.* **2014**, *14*, 5792; b) S. Fleischer, M. Shevach, R. Feiner, T. Dvir, *Nanoscale* **2014**, *6*, 9410; c) K. Baranes, M. Shevach, O. Shefi, T. Dvir, *Nano Lett.* **2016**, *16*, 2916; d) T. Dvir, B. P. Timko, M. D. Brigham, S. R. Naik, S. S. Karajanagi, O. Levy, H. Jin, K. K. Parker, R. Langer, D. S. Kohane, *Nat. Nanotechnol.* **2011**, *6*, 720.
- [11] a) S. Fleischer, R. Feiner, A. Shapira, J. Ji, X. Sui, H. D. Wagner, T. Dvir, *Biomaterials* **2013**, *34*, 8599; b) S. Fleischer, A. Shapira, O. Regev, N. Nseir, E. Zussman, T. Dvir, *Biotechnol. Bioeng.* **2014**, *117*, 1246; c) S. Fleischer, J. Miller, H. Hurowitz, A. Shapira, T. Dvir, *Nanotechnology* **2015**, *26*, 291002; d) G. C. Engelmayer, M. Cheng, C. J. Bettinger, J. T. Borenstein, R. Langer, L. E. Freed, *Nat. Mater.* **2008**, *7*, 1003; e) M. E. Kolewe, H. Park, C. Gray, X. Ye, R. Langer, L. E. Freed, *Adv. Mater.* **2013**, *25*, 4459.
- [12] M. Shevach, N. Soffer-Tsur, S. Fleischer, A. Shapira, T. Dvir, *Biofabrication* **2014**, *6*, 024101.
- [13] a) H. Park, B. L. Larson, M. E. Kolewe, G. Vunjak-Novakovic, L. E. Freed, *Exp. Cell Res.* **2014**, *321*, 297; b) L. L. Chiu, M. Radisic, *Biomaterials* **2010**, *31*, 226; c) Y. Miyagi, L. L. Chiu, M. Cimini, R. D. Weisel, M. Radisic, R.-K. Li, *Biomaterials* **2011**, *32*, 1280.
- [14] G. Vunjak-Novakovic, N. Tandon, A. Godier, R. Maidhof, A. Marsano, T. P. Martens, M. Radisic, *Tissue Eng., Part B* **2010**, *16*, 169.
- [15] M. Tomaske, B. Gerritse, L. Kretzers, R. Pretre, A. Dodge-Khatami, M. Rahn, U. Bauersfeld, *Ann. Thorac. Surg.* **2008**, *85*, 1704.
- [16] a) D.-H. Kim, Y.-S. Kim, J. Amsden, B. Panilaitis, D. L. Kaplan, F. G. Omenetto, M. R. Zakin, J. A. Rogers, *Appl. Phys. Lett.* **2009**, *95*, 133701; b) J. A. Rogers, T. Someya, Y. Huang, *Science* **2010**, *327*, 1603; c) D. H. Kim, N. Lu, R. Ma, Y. S. Kim, R. H. Kim, S. Wang, J. Wu, S. M. Won, H. Tao, A. Islam, K. J. Yu, T. I. Kim, R. Chowdhury, M. Ying, L. Xu, M. Li, H. J. Chung, H. Keum, M. McCormick, P. Liu, Y. W. Zhang, F. G. Omenetto, Y. Huang, T. Coleman, J. A. Rogers, *Science* **2011**, *333*, 838; d) H. J. Chung, M. S. Sulkin, J. S. Kim, C. Goudeseune, H. Y. Chao, J. W. Song, S. Y. Yang, Y. Y. Hsu, R. Ghaffari, I. R. Efimov, J. A. Rogers, *Adv. Healthcare Mater.* **2014**, *3*, 59; e) G. Hong, T.-M. Fu, T. Zhou, T. G. Schuhmann, J. Huang, C. M. Lieber, *Nano Lett.* **2015**, *15*, 6979; f) C. Xie, J. Liu, T.-M. Fu, X. Dai, W. Zhou, C. M. Lieber, *Nat. Mater.* **2015**, *14*, 1286; g) X. Dai, W. Zhou, T. Gao, J. Liu, C. M. Lieber, *Nat. Nanotechnol.* **2016**, *11*, 96; h) T.-M. Fu, G. Hong, T. Zhou, T. G. Schuhmann, R. D. Viveros, C. M. Lieber, *Nat. Methods* **2016**, *13*, 875; i) T. G. Schuhmann Jr., G. Thomas, J. Yao, G. Hong, T.-M. Fu, C. M. Lieber, *Nano Lett.* **2017**, *17*, 5836.
- [17] L. Xu, S. R. Gutbrod, A. P. Bonifas, Y. Su, M. S. Sulkin, N. Lu, H. J. Chung, K. I. Jang, Z. Liu, M. Ying, C. Lu, R. C. Webb, J. S. Kim, J. I. Laughner, H. Cheng, Y. Liu, A. Armeen, J. W. Jeong, G. T. Kim, Y. Huang, I. R. Efimov, J. A. Rogers, *Nat. Commun.* **2014**, *5*, 3329.
- [18] X. Dai, W. Zhou, T. Gao, J. Liu, C. M. Lieber, *Nat. Nanotechnol.* **2016**, *11*, 776.
- [19] T. Zhou, G. Hong, T.-M. Fu, X. Yang, T. G. Schuhmann, R. D. Viveros, C. M. Lieber, *Proc. Natl. Acad. Sci. USA* **2017**, *114*, 5894.
- [20] J. Liu, T.-M. Fu, Z. Cheng, G. Hong, T. Zhou, L. Jin, M. Duvvuri, Z. Jiang, P. Kruskal, C. Xie, *Nat. Nanotechnol.* **2015**, *10*, 629.
- [21] R. Feiner, T. Dvir, *Nat. Rev. Mater.* **2017**, *3*, 17076.
- [22] P. Cai, B. Hu, W. R. Leow, X. Wang, X. J. Loh, Y.-L. Wu, X. Chen, *Adv. Mater.* **2018**, *30*, 1800572.

- [23] B. Tian, J. Liu, T. Dvir, L. Jin, J. H. Tsui, Q. Qing, Z. Suo, R. Langer, D. S. Kohane, C. M. Lieber, *Nat. Mater.* **2012**, *11*, 986.
- [24] R. Feiner, S. Fleischer, A. Shapira, O. Kalish, T. Dvir, *J. Controlled Release* **2018**, *281*, 189.
- [25] R. Feiner, L. Engel, S. Fleischer, M. Malki, I. Gal, A. Shapira, Y. Shacham-Diamand, T. Dvir, *Nat. Mater.* **2016**, *15*, 679.
- [26] a) D. Allen, S. Kurihara, *J. Physiol.* **1982**, *327*, 79; b) M. Carlsson, P. Cain, C. Holmqvist, F. Stahlberg, S. Lundback, H. Arheden, *Am. J. Physiol.: Heart Circ. Physiol.* **2004**, *287*, H243.
- [27] M. Pyo, J. R. Reynolds, *Chem. Mater.* **1996**, *8*, 128.
- [28] R. Wadhwa, C. F. Lagenaur, X. T. Cui, *J. Controlled Release* **2006**, *110*, 531.
- [29] D. Ge, X. Tian, R. Qi, S. Huang, J. Mu, S. Hong, S. Ye, X. Zhang, D. Li, W. Shi, *Electrochim. Acta* **2009**, *55*, 271.
- [30] S. Geetha, C. R. Rao, M. Vijayan, D. Trivedi, *Anal. Chim. Acta* **2006**, *568*, 119.
- [31] a) E. Figueredo, J. Cuesta-Herranz, M. De Las Heras, M. Lluch-Bernal, A. Umpierrez, J. Sastre, *Allergy* **1997**, *52*, 877; b) S. Neff, F. Stapelberg, A. Warmington, *Anaesth. Intensive Care* **2002**, *30*, 370.
- [32] N. Calonge, D. B. Petitti, T. G. DeWitt, L. Gordis, K. D. Gregory, R. Harris, G. Isham, M. L. LeFevre, C. Loveland-Cherry, L. N. Marion, *Ann. Intern. Med.* **2009**, *150*, 221.
- [33] M. Imazio, Y. Adler, *Heart Failure Rev.* **2013**, *18*, 355.
- [34] a) B. Zinger, L. L. Miller, *J. Am. Chem. Soc.* **1984**, *106*, 6861; b) R. Sivakumar, P. V. A. Babu, C. S. Shyamaladevi, *Chem.-Biol. Interact.* **2008**, *176*, 227.
- [35] J. W. Mason, *N. Engl. J. Med.* **1987**, *316*, 455.
- [36] A. J. Pope, G. B. Sands, B. H. Smaill, I. J. LeGrice, *Am. J. Physiol.: Heart Circ. Physiol.* **2008**, *295*, H1243.
- [37] Y. Zhang, H. Ouyang, C. T. Lim, S. Ramakrishna, Z. M. Huang, *J. Biomed. Mater. Res., Part B* **2005**, *72*, 156.
- [38] R. Edri, I. Gal, N. Noor, T. Harel, S. Fleischer, N. Adadi, O. Green, D. Shabat, L. Heller, A. Shapira, *Adv. Mater.* **2019**, *31*, 1803895.
- [39] N. Bursac, M. Papadaki, R. Cohen, F. Schoen, S. Eisenberg, R. Carrier, G. Vunjak-Novakovic, L. Freed, *Am. J. Physiol.: Heart Circ. Physiol.* **1999**, *277*, H433.
- [40] C. Dagdeviren, B. D. Yang, Y. Su, P. L. Tran, P. Joe, E. Anderson, J. Xia, V. Doraiswamy, B. Dehdashti, X. Feng, B. Lu, R. Poston, Z. Khalpey, R. Ghaffari, Y. Huang, M. J. Slepian, J. A. Rogers, *Proc. Natl. Acad. Sci. USA* **2014**, *111*, 1927.
- [41] a) G. Zheng, F. Patolsky, Y. Cui, W. U. Wang, C. M. Lieber, *Nat. Biotechnol.* **2005**, *23*, 1294; b) F. Patolsky, G. Zheng, C. M. Lieber, *Nat. Protoc.* **2006**, *1*, 1711.